17th World Conference on Earthquake Engineering, 17WCEE
Sendai, Japan - September 13th to 18th 2020

The FM-IBEM solution to the scattering of seismic waves by local sites in a fluid-saturated poroelastic half-space

Zhongxian Liu [(1)], Chenrui He[(2)], XiangHui Zeng[(3)] ,Shuaijie Sun[(4)]

[(1)] *Professor, Tianjin Key Laboratory of civil structure protection and reinforcement, Tianjin Chengjian University, Tianjin 300384, China, zhongxian1212@163.com*
[(2)] *Tianjin Key Laboratory of civil structure protection and reinforcement, Tianjin Chengjian University, Tianjin 300384, China*
[(3)] *Tianjin Binhai New Area Construction and Investment Rail Transit Construction Co., Tianjin 300384, China*
[(4)] *Hohai University, Nanjing 210098, China*

Abstract

The fast multi-pole indirect boundary element method (FM-IBEM) is proposed to efficiently solve the high-frequency and large-scale scattering of seismic waves by complex local sites under fluid-saturated poroelastic heterogeneous medium. The Graf addition theorem and the plane wave expansion theory, corresponding to 2-D solution and 3-D solution respectively, are utilized to solve the theoretical expansion formulas of fast multi-pole method. The bottleneck of dense matrix can be broken by replacing the coefficient matrix with a tree structure. Thus, the memory requirement and the CPU time for solving the system can be drastically reduced compared to the conventional indirect boundary element method, especially for the solution of high-frequency and multi-body wave scattering. Through the study of seismic motion in typical local sites, the effects of important parameters, including the incident wave frequency, incident angle, medium porosity and boundary drainage conditions, are discussed.

Keywords: The fast multi-pole boundary element method (FM-IBEM); Scattering of seismic waves; Fluid-saturated poroelastic heterogeneous medium; Seismic motion

1. Introduction

The wave propagation and diffraction excited by the subsurface scatterers, such as canyons, cavity and cracks, in fluid-saturated poroelastic medium play a great role in various filed such as in earthquake engineering, oil and gas exploration, geophysics, civil engineering and other fields. Among the most frequently employed models is the dynamic poroelasticity theory developed by Biot ([1, 2, 3]), which successfully predicts the slow compressional wave and the frequency dependent attenuation and dispersion of waves in fluid-saturated poroelastic medium.

The calculation for wave motion in poroelastic medium can be based on analytical solutions and numerical methods. Analytical methods are usually based on the wave function expansion [4, 5, 6]. Numerical methods include the finite element method [7, 8], the finite difference method [9, 10, 11], spectral element method [12], boundary element method (BEM) [13, 14, 15, 16], discrete wave number method, and other boundary-type or hybrid methods [17]. However, it should be noted that the method mentioned above, used to simulate the propagation and scattering of elastic waves in fluid-saturated poroelastic medium, is not so effective or efficient for the large-scale and high-frequency problems.

Thus, in recent years, many studies have been focused on improving the traditional BEM through fast algorithms. In this context, the fast multipole boundary element method (FM-IBEM), which can significantly reduce computational complexity and memory requirements, has great advantages and has become increasingly popular in recent years [18, 19, 20, 21]. Previous FM-IBEM studies were all based on single-phase materials, such as solids or fluids.

This paper is aimed at extending the previous work of the FM-IBEM developed by Liu et al. [20] for elastic waves to fluid-saturated porous medium. The developed methodology can efficiently solve 2-D and 3-D large-scale or high-frequency wave scattering problems in a poroelastic unbounded domain. It can also be used to solve vibration problems in two-phase porous medium, such as soil-structure dynamic interaction, vibration isolation design in saturated site, etc.

The main content of the paper is as follows. In Section 2, the computational process of FM-IBEM is briefly introduced, including the process of expansion and the path of delivery. In Section 3, the numerical accuracy and efficiency are verified by comparing with the existing results. In Section 4, the scattering of elastic waves in classical sites is solved, and the effects of different parameters are discussed. Finally, Section 5 draws several important conclusions.

2. The FM-IBEM

According to the IBEM, the wave field consists of the scattered wave field and the free field. In a fluid-saturated poroelastic medium, the former can be obtained by imposing the virtual loads of forces in each direction and fluid source on the surface of the discrete element. Considering boundary conditions, the densities of the virtual loads are obtained by solving the discretized integral equations. Finally, the solution can be constructed by the superposition of the free field and the scattered field solutions.

In the traditional IBEM, Gauss-Jordan elimination and iterative methods such as GMRES usually be adopt to solve the fully-populated integral equations, and the solving time require $O(N^3)$ and $O(N^2)$, respectively. In the computational process, the equations matrixes will generate $O(N^3)$ memory storage. These defects affect the application of the BEM in actual large-scale and high-frequency wave scattering issues. Thus the FM-IBEM should be adopted to overcome these disadvantages.

The crucial steps of the FM-IBEM are expansions and translations of Green's functions. Through these processes, element-to-element connections are transformed to cell-to-cell connections. Experimental result shows that the magnitude and time of computation are reduced dramatically and the efficiency increases greatly by using this method.

2.1 Tree structure construction

Element discretization in FM-IBEM is the same as that in BEM. Take a 2-D problem as an example, a large enough square is needed to set up to surround all elements discretized in the previous step (the cell of level 0). Then this parent square is divided into four equal sub-squares (the cell of level 1). Continue to divide the square by this method until the minimum square meets the requirement for the number of elements included. The last step is to delete the squares without any unit integral point. A quad-tree structure is constructed after these processes. For 3-D field, cube is used instead of square for the same steps as in 2-D, and then the octree structure can be obtained. The cell without subset is called leaf cell, and the cell in its upper levels is called parent cell.

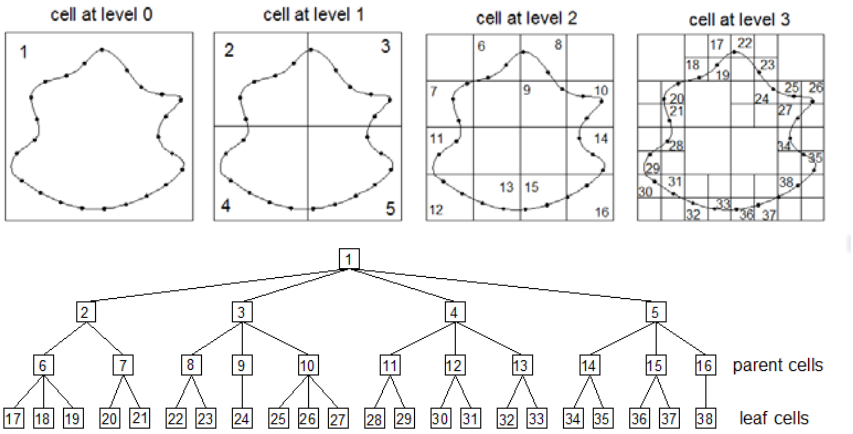

Fig.1 Quad-tree structure and its construction [22]

With the help of GMRES method, the coefficient matrix is replaced by a tree structure in the process of iteration, multiplied by the iteration quantity, and the coefficient matrix does not need to be displayed and stored.

2.2 The FMM expansion and translation

Figure 2 illustrates the basic principles of the fast multipole boundary element method. Now assume y is the source point and x is the field point, y_0 and x_0 correspond to the center of the leaf cells, y_c and x_c correspond to the center of the parent cells, respectively, which satisfies $|y - y_0| \leq |x - y_0|/2$. The process that transforms the influence of virtual loads at point y to y_0 is called the multipole expansion. Correspondingly, the processes from y_0 to y_c, y_c to x_c, x_c to x_0 and x_0 to x are called shift of multipole to multipole moments, shift of multipole to local moments, shift of local to local moments and local expansion, respectively.

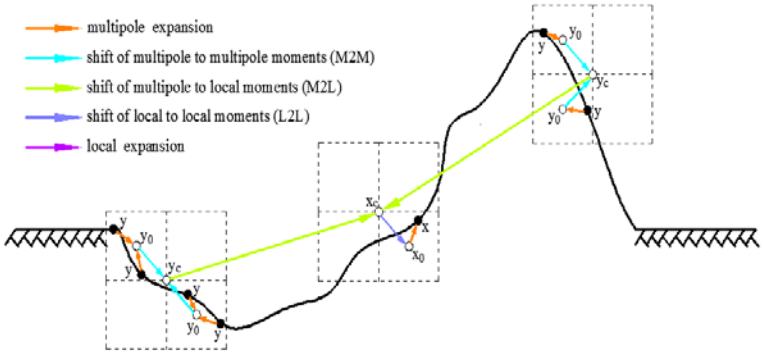

Fig. 2 The basic diagram of the fast multi-pole boundary element method [23]

The Graf addition theorem is applied in a 2-D case.

$$Z_v(r)e^{iv\alpha} = \sum_{n=-\infty}^{\infty} Z_{v-n}(r_1)e^{i(v-n)\gamma} J_n(r_2)e^{in\beta} \tag{1}$$

in which, Z represents three kinds Bessel functions, including J, Y, H; n is the truncation term used to control precision, and it can be determined by empirical formula given in Eq.(2) (Sakuma and Yasuda [24]); in terms of numerical, $r_2 < r_1$ is required (if $Z=J$, this restriction can be ignored). Other symbols are shown in Fig.3.

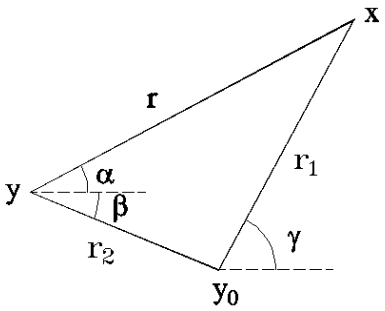

Fig.3 Plane parameters in the Graf addition theorem [22]

$$n = kL + c\log(kL + \pi) \tag{2}$$

where L is the length of leaf or parent cell, c is a parameter to control precision. The expansion and application of kernel function can be found in the work of Liu et al.[22].

Following the plane wave expansion theory , [25], the multipole expansion of 3-D poroelastic wave potential function can be expressed as:

$$f(q,r) = \frac{\mathrm{i}q}{2(2p+1)} \sum_{n=0}^{p} \sum_{m=0}^{2p} \omega_n R_n^m(q, \boldsymbol{yy}_0)\, T_n^m(q, \boldsymbol{y}_0\boldsymbol{x}_0)\, S_n^m(q, \boldsymbol{x}_0\boldsymbol{x}) \tag{3}$$

$$R_n^m(q, \boldsymbol{yy}_0) = e^{\mathrm{i}q(\boldsymbol{y}_0 - \boldsymbol{y})\cdot\hat{\boldsymbol{k}}_n^m} \tag{4}$$

$$S_n^m(q, \boldsymbol{x}_0\boldsymbol{x}) = e^{\mathrm{i}q(\boldsymbol{x}-\boldsymbol{x}_0)\cdot\hat{\boldsymbol{k}}_n^m} \tag{5}$$

$$T_n^m(q, \boldsymbol{y}_0\boldsymbol{x}_0) = \sum_{l=0}^{p} \mathrm{i}^l (2l+1) h_l^{(2)}(qr) P_l(\hat{\boldsymbol{r}}\cdot\hat{\boldsymbol{k}}_n^m) \tag{6}$$

where， $\hat{k}_n^m = (\sin\theta_n\cos\phi_m, \sin\theta_n\sin\phi_m, \cos\theta_m)$, $\theta = a\cos x_n$, $\phi_m = 2\pi m/(2p+1)$, x_n and ω_n are the horizontal coordinates and weight coefficients of Gaussian quadrature in [-1,1], $\hat{\boldsymbol{r}} = \overrightarrow{y_0x_0}/|\hat{\boldsymbol{r}}|$ and $r = |\hat{\boldsymbol{r}}|$, and they need to satisfy $|\overrightarrow{yy_0}| < |\overrightarrow{y_0x_0}|$ and $|\overrightarrow{x_0x}| < |\overrightarrow{y_0x_0}|$. And the truncation term can be determined by empirical formula as [24]:

$$p = 2kR + c_0 \log(2kR + \pi) \tag{7}$$

in which, k is wave number, R and c_0 are the circumcircle radius of a tree structure and precision control parameter, respectively. Refer to Liu et al. [23] for detailed process of calculation.

3. Numerical accuracy and computational efficiency

3.1 Verification of accuracy for the FM-IBEM

To examine the numerical accuracy of FM-IBEM, verification will be performed as follow: comparing the 2-D scattering of a plane P_1 wave by a semi-circular canyon in poroelastic half-space calculated by FM-IBEM and IBEM.

Fig.4 shows the 2-D scattering of plane P_1 wave by a semi-circular canyon with drained surface in a fluid-saturated poroelastic half-space calculated by FM-IBEM and IBEM used in the work of Liang et al. [26]. The parameters are using dimensionless frequencies η=0.5, 10, with the medium porosities n=0.3; Poisson's ratio v=0.25, the angle of incidence θ=π/2, while the residual convergence $\varepsilon = 10^{-3}$, and the hysteretic damping ratio is set as ξ=0.001. The results of the two methods are consistent, which indicates that FM-IBEM has sufficient accuracy. Thus, FM-IBEM prospered in this paper can be widely used.

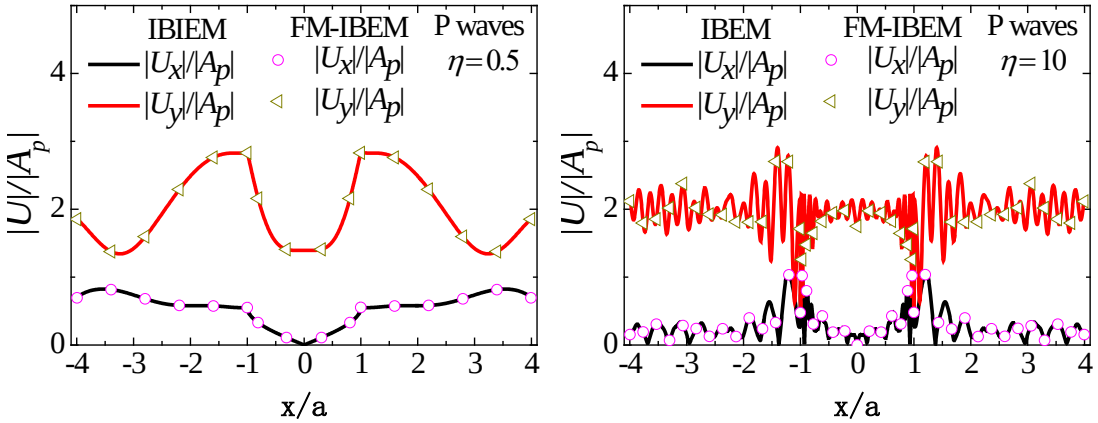

Fig.4 Comparison between the displacement amplitudes around a semi-circular canyon by FM-IBEM and that of IBEM [22]

3.2 Computational efficiency and memory requirement

In order to verify the superiority of FM-IBEM in the calculation in a poroelastic half-space, the scattering of plane P_1 wave by a semi-circle canyon is considered. Set the dimensionless frequency η=1.0, porosity n=0.3 and the number of elements N=901-6,501 (*DOFs*=1,802-13,002).

Fig.5 (a) and Fig.5 (b) display the total CPU time varying with degrees of freedom for FM-IBEM and IBEM. When *DOFs*=13002, the total CPU time reaches 193528s (about 54h), and the memory is more than

13GB. However, for the FM-IBEM, the CPU time increases approximately linearly along with the *DOFs*. When *DOFs*=13002, the requirement of total CPU time and memory capacity are reduced significantly by using FM-IBEM, with only 431s and 0.45 GB .Therefore, compared with IBEM, FM-IBEM reduces both computation time and memory capacity, which lays a foundation for the fast solution of broadband scattering or large-scale issues in a fluid-saturated poroelastic half-space.

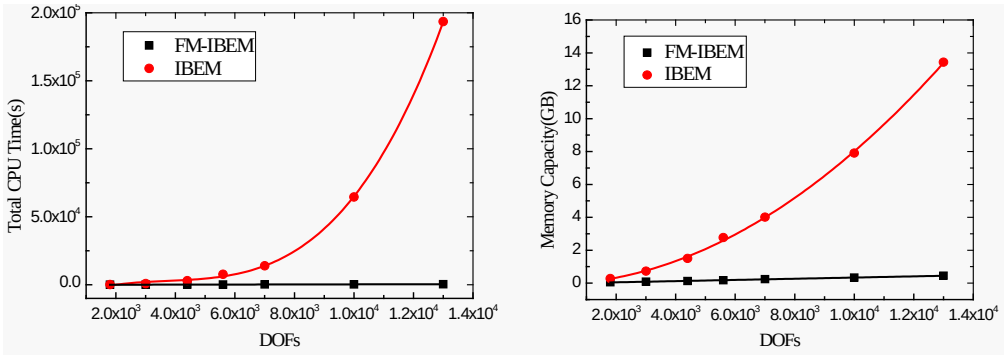

(a)Comparison of the total CPU time (b) Comparison of the memory capacity

Fig.5 Comparison of the total CPU time and memory capacity between FM-IBEM and IBEM [22]

4. Numerical results and discussion

In this Section, the proposed FM-IBEM method is applied to solve the broadband scattering of plane waves by local sites in a fluid-saturated poroelastic medium, which have significance in seismic wave analysis, nondestructive testing, geo-prospecting, etc. We shall examine the influences of the incident angle, frequency, porosity, and the permeable or impermeable condition of the boundary.

Referring to Lin et al. [27], the parameters adopted are as follows: Poisson's ratio v=0.25; critical porosity n_{cr}=0.36; critical bulk modulus of the solid skeleton k_{cr}=200MPa; bulk modulus of the solid grain k_g=36,000MPa; bulk modulus of fluid k_f=2,000MPa; mass density of the solid grain ρ_g =2,650kg/m^3; mass density of fluid ρ_f =1,000kg/m^3.

4.1 The broadband scattering of elastic waves by a semi-circle canyon in a fluid-saturated poroelastic half-space

The model is shown in Figure 6. In order to study the broadband scattering phenomenon of elastic wave by a semicircle canyon, P_1 wave and SV wave are selected as incident waves with the dimensionless frequency η=1, 5, 10, 25, and the incident angle is set as θ=π/2. The final displacement amplitudes are normalized by the displacement amplitude of the incident waves. For P_1 wave incident with the dimensionless frequency η=25, it should be noted that the GMRES iteration steps are 165, 102, 101 and 84 corresponding to the porosity n=0.1, 0.3, 0.34 and 0.36, respectively, and the total CPU time is about 20-25 minutes by the application of the FM-IBEM.

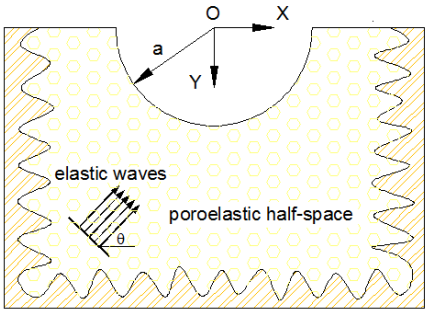

Fig.6 Calculation model for 2-D scattering of elastic waves by a semi-circle canyon in a poroelastic half-space

Fig.7 and Fig.8 illustrate the results of displacement amplitudes around a semi-circle canyon in a fluid-saturated poroelastic half-space at different frequencies when the P_1 and SV waves are vertically incident, respectively. Through observation and comparison, it can be seen that the effect of frequency on the scattering of waves is significantly. With the increase of frequency, the spatial variation of displacement amplitude becomes more drastically. The numerical results reveal that the peak of displacement amplitude often appears around the corner of the semicircle canyon (x/a= -1) which is due to the focusing effect of the elastic wave at the corner of the canyon caused by diffraction effect. For the high frequency, such as η=25, the bottom of the canyon is similar to a horizontal surface. Therefore, the diffraction effect becomes inconspicuous, and the displacement amplitude at the bottom of the canyon is closed to that of horizontal surface in the free field. In addition to the bottom of the canyon, there is a special phenomenon on the horizontal ground surface that the displacement amplitude converges to the free field displacement amplitude as the frequency increases.

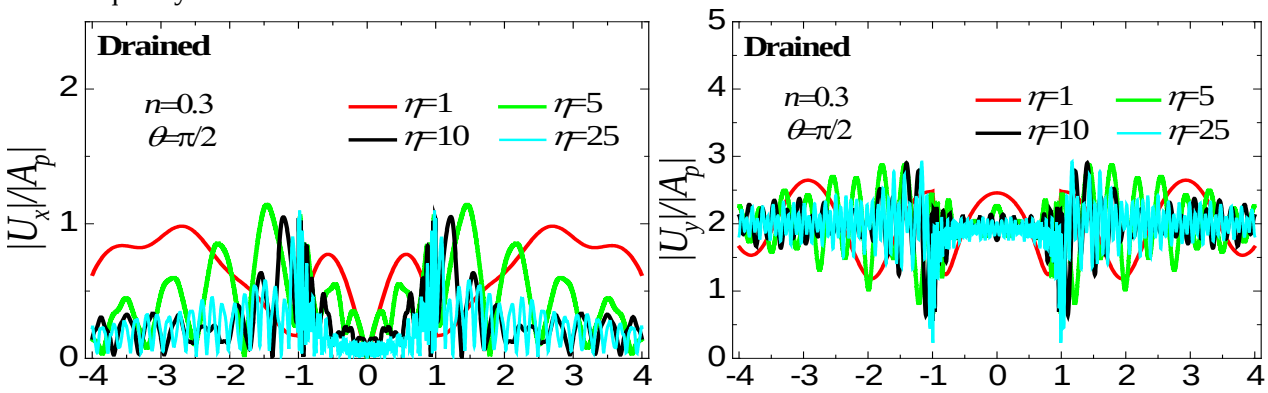

Fig.7 The displacement amplitudes of P_1 wave with different frequencies incident around a semi-circle canyon in a fluid-saturated poroelastic half-space

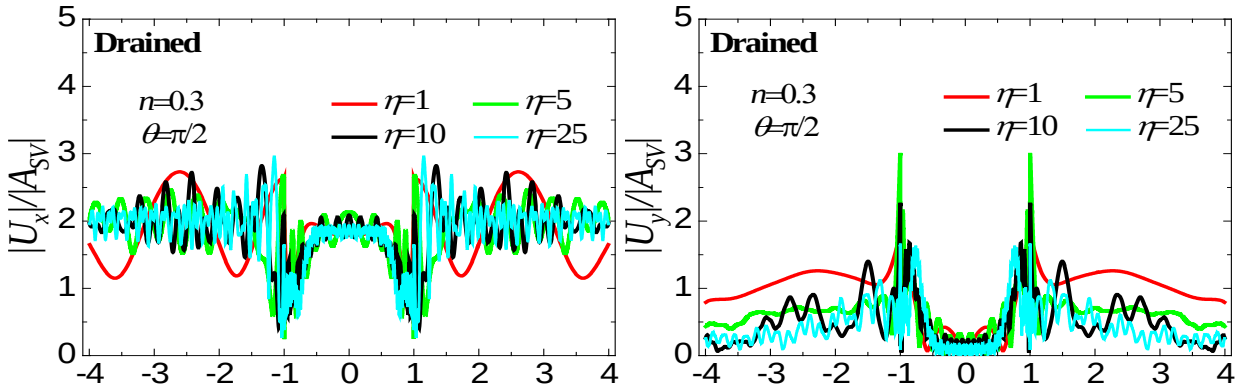

Fig.8 The displacement amplitudes of SV wave with different frequencies incident around a semi-circle canyon in a fluid-saturated poroelastic half-space

4.2 The 2-D scattering of P_1 wave by cracks in a fluid-saturated poroelastic half-space

The model is shown in Fig.9. Define the major axis of the crack as a, and the minor axis semi-diameter as b. In order to study the effect of cracks on the scattering of P_1 wave in a fluid-saturated poroelastic half-space, a single crack placed horizontally with a circumference ratio a/b=10 and the depth d=2a is taken as an example. Set the drainage condition is drained.

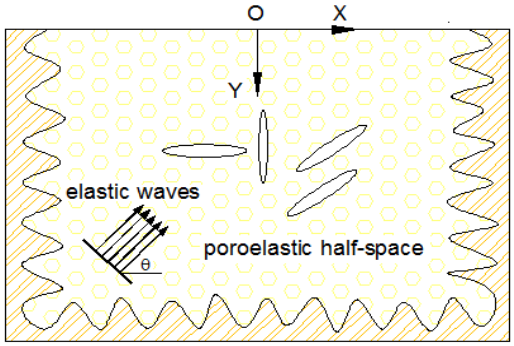

Fig.9 Calculation model for 2-D scattering of elastic waves by cracks in a poroelastic half-space

Fig.10 and Fig.11 show the displacement amplitudes at different frequencies (η=1, 3, 5) and porosities (n=0.1, 0.3, 0.34, 0.36). Through observation and comparison, it can be seen that the scattering of wave is not only affected by frequency, but also by porosity and the angle of incidence. When the porosity gradually approaches the critical porosity (n=0.36), the spatial variation of surface displacement is more complicated. When the P_1 wave is incident obliquely, the horizontal displacement amplitude changes are greater than the vertical displacement amplitude. It means that the horizontal displacement amplitude is greatly affected by the porosity and increases with frequency.

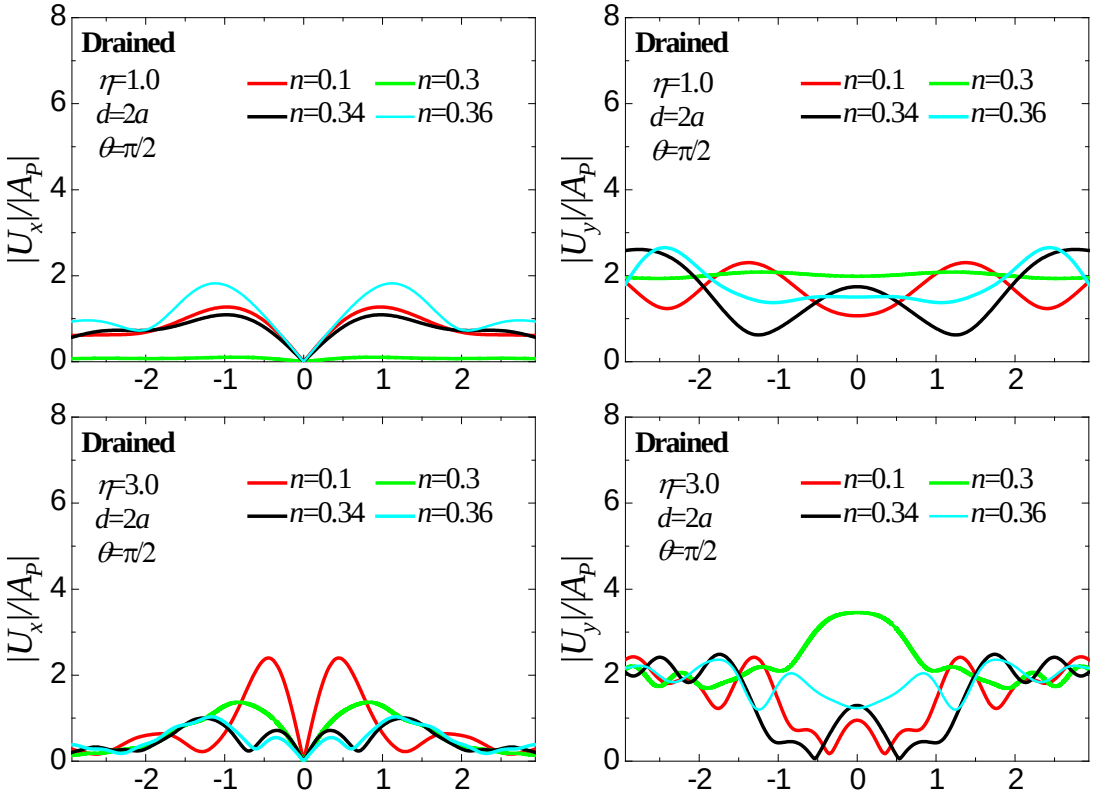

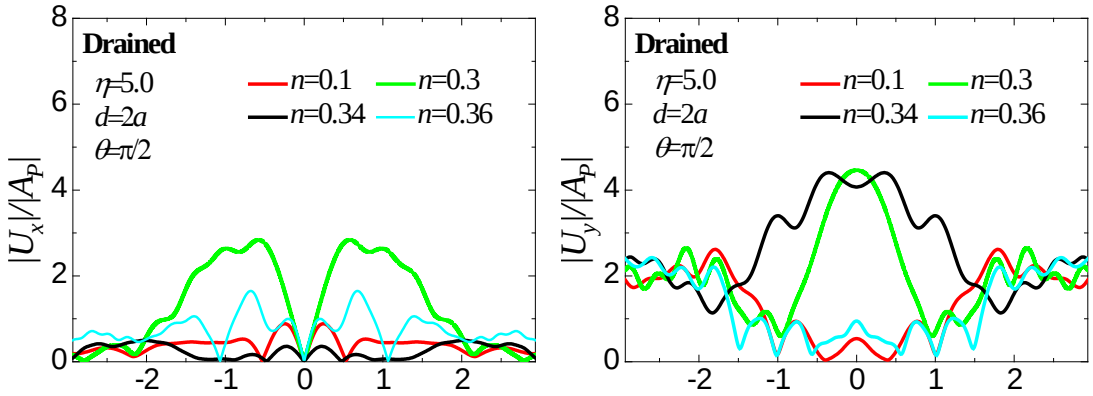

Fig.10 The displacement amplitudes of P_1 wave with different frequencies incident around a crack in a fluid-saturated poroelastic half-space (θ=0)

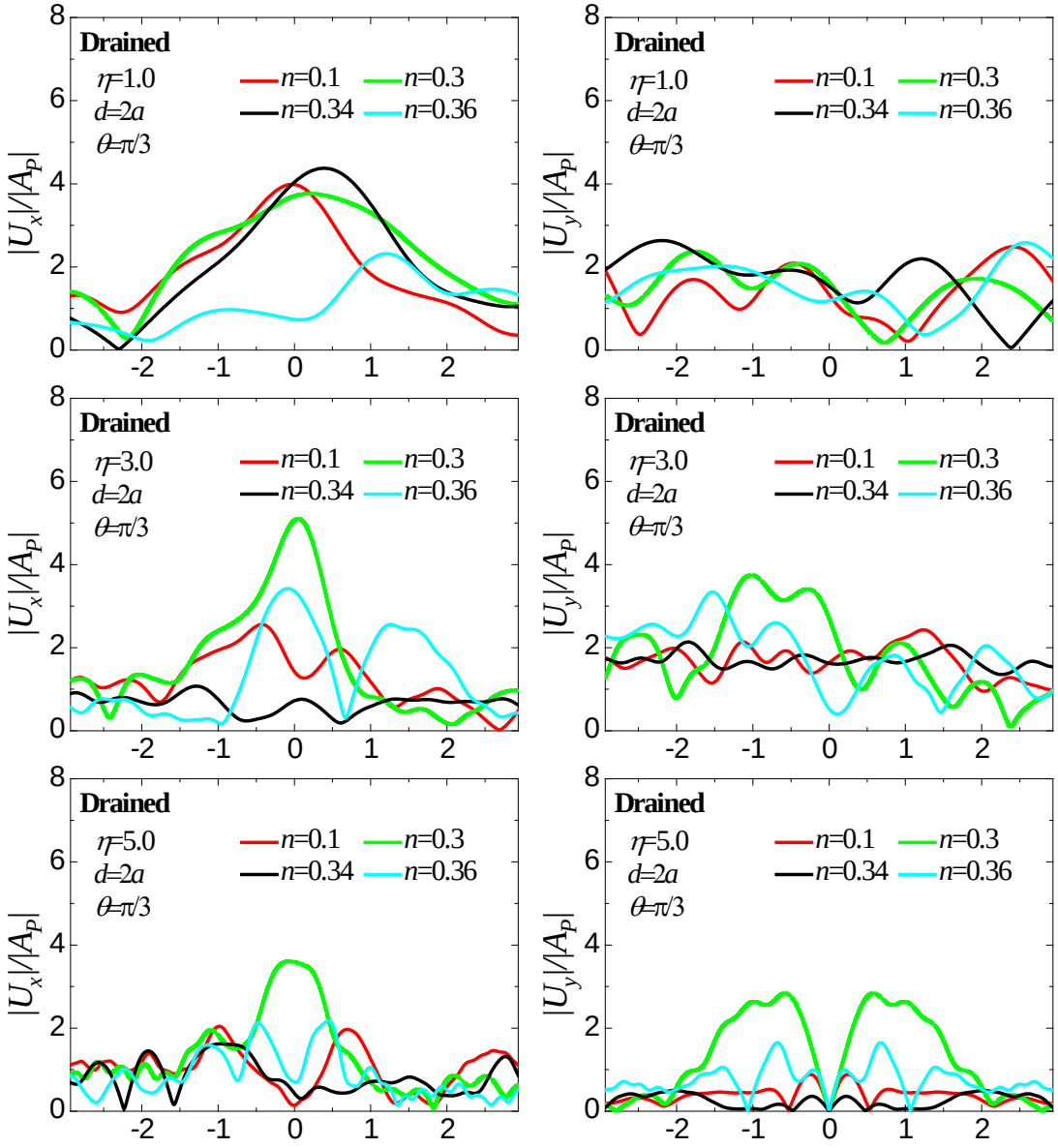

Fig.11 The displacement amplitudes of P_1 wave with different frequencies incident around a crack in a fluid-saturated poroelastic half-space (θ=π/6)

4.3 The broadband scattering of plane P_1 wave by a semi-spherical canyon in a poroelastic half space

The calculation model is given in Fig.12. The semi-spherical canyon surface is assumed to be drained. Fig.2 shows the displacement amplitudes of section A (x=0) under incident plane P_1 wave. Where, the parameters are selected as n=0.3, θ=0 and π/6, η=1, 5 and 10. Section A is selected as output section.

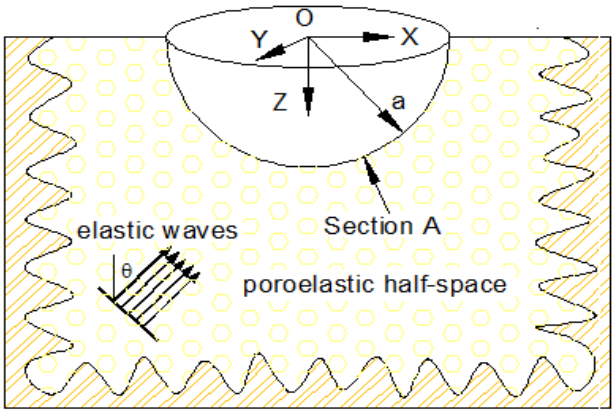

Fig.12 Calculation model for 3-D scattering of elastic waves by a semi-spherical canyon in a poroelastic half-space

The results given in Fig.13 show that the peak displacement amplitude usually occurs at the corner of the canyon for low-frequency P_1 waves due to the wave focusing effect. However, with the increase of incident frequency, the amplification effect also appears at the bottom of the canyon. These are consistent with the results in Section 4.1. We also observe that the seismic responses of the 3-D canyon under vertically incident P_1 waves (θ_a =0°) is different from that of oblique incidence (θ_a =30°)in the spatial distribution. Also, the vertical displacement amplitude for θ_a =0° is similar to that of the oblique incidence, but the latter can generate significant amplification effect on the horizontal displacement amplitude. Moreover, under the obliquely incident wave, due to the shielding effect of the canyon, surface displacement responses on the right of the canyon is smaller than that on the left of the canyon.

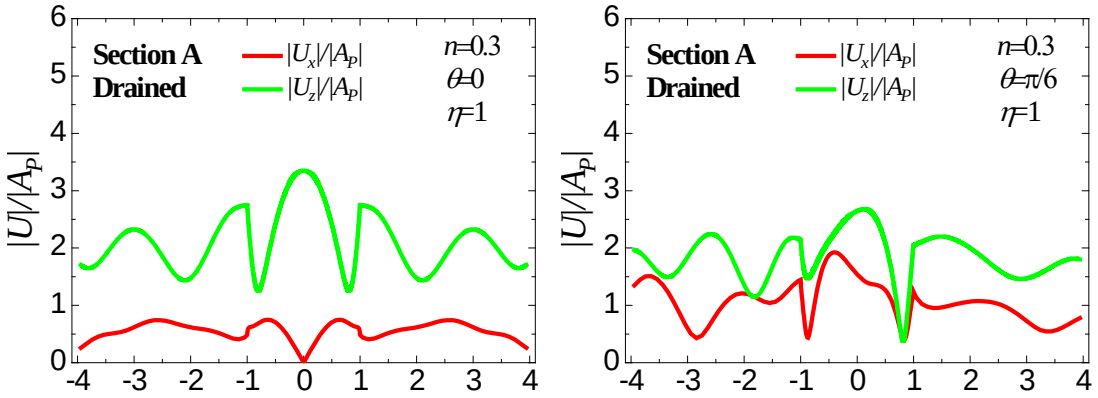

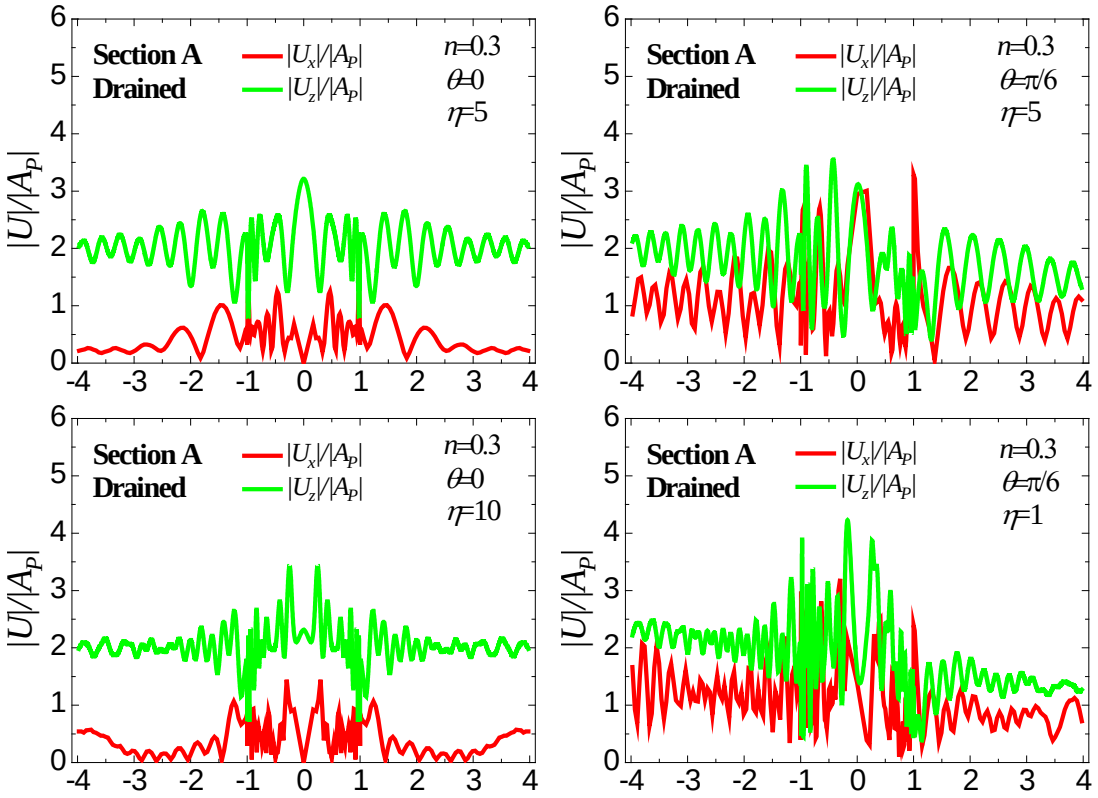

Fig.13 The displacement amplitudes of P_1 wave with different frequency and angel around a semi-spherical canyon in a poroelastic half space

5. Conclusions

The fast multi-pole boundary element method (FM-IBEM) that combines the fast multi-pole method with indirect boundary element method (BEM) is developed to solve seismic wave motion in a fluid-saturated poroelsatic half space. The broadband and efficient solution of the scattering of elastic waves by local sites in a fluid-saturated poroelastic half-space is realized , which supplies a good reference case for other numerical methods. Numerical results demonstrated that this proposed method effectively breaks through the bottleneck of the dense matrix characteristic in solving large-scale and high-frequency problems and greatly improve the computing efficiency of traditional BEM. Through the simulation and analysis for typical local sites such as a semi-circle canyon, crack and a group of cracks in 2-D half-space, and a semi-spherical canyon in 3-D half-space, the wave focusing effect and amplification effect under different topographic conditions due to the mechanism of elastic wave diffraction and coherence are clearly revealed. The scattering of elastic waves in a fluid-saturated poroelastic mediums strongly dependent of the incident wave frequency, incident angle, medium porosity, and boundary drainage conditions. Whether in 2-D or 3-D half-space, canyon will cause an amplification effect of displacement amplitude, and the effect is more obvious at the corner of the canyon. In addition, the existence of a group of cracks and spherical cavities shows the isolation effect on the half-space surface motion, especially for vertical displacement amplitude, and the effect becomes more obvious with the increasing of incident frequency. The results are helpful to deeply understand the seismic wave propagation and scattering in fluid-saturated poroelastic medium. It is significantly important to seismic fortification in fluid-saturated complex sites in urban areas

6. Acknowledgements

This work was supported by the National Natural Science Foundation of China under grants (51678390), Tianjin Key Research Program of Application Foundation Advanced Technology (18JCZDJC39200), and Tianjin city science and technology support program (17YFZCSF01140).

7. References

[1] Biot MA (1956): Theory of propagation of elastic waves in a fluid-saturated porous solid. 1. Low-frequency range. *The Journal of the acoustical Society of America*, 28(2):168-178

[2] Biot MA (1956): Theory of propagation of elastic waves in a fluid‐saturated porous solid. II. Higher frequency range. *The Journal of the acoustical Society of America*, 28(2), 179-191.

[3] Biot MA (1962): Mechanics of deformation and acoustic propagation in porous media. *Journal of applied physics*, 33(4), 1482-1498.

[4] Zimmerman C, Stern M (1993): Scattering of plane compressional waves by spherical inclusions in a poroelastic medium. *The Journal of the Acoustical Society of America*, 94(1), 527-536.

[5] Liang JW, Ba ZN, Lee VW (2006): Diffraction of plane SV waves by a shallow circular-arc canyon in a saturated poroelastic half-space. *Soil dynamics and earthquake engineering*, 26(6-7), 582-610.

[6] Cui CY, Zhang SP, Meng K, Xu CS, Yang G (2018): An analytical solution for integrity detection of a floating pile embedded in saturated viscoelastic half-space. *International Journal of Distributed Sensor Networks*, 14(9), 1-8.

[7] Shi L, Wang P, Cai Y, Cao, Z (2016): Multi-transmitting formula for finite element modeling of wave propagation in a saturated poroelastic medium. *Soil Dynamics and Earthquake Engineering*, 80, 11-24.

[8] Li PJ, Yuan XK (2020): Convergence of an adaptive finite element DtN method for the elastic wave scattering by periodic structures. *Computer Methods in Applied Mechanics and Engineering*, 360, 112722.

[9] Masson YJ, Pride SR (2010): Finite-difference modeling of Biot's poroelastic equations across all frequencies. *Geophysics*, 75(2), N33-N41.

[10] Blanc E, Chiavassa G, Lombard B (2013): A time-domain numerical modeling of two-dimensional wave propagation in porous media with frequency-dependent dynamic permeability. *The Journal of the Acoustical Society of America*, 134(6), 4610-4623.

[11] Yang SB, Bai CY, Greenhalgh S (2020): Seismic wavefield modelling in two-phase media including undulating topography with the modified Biot/squirt model by a curvilinear-grid finite difference method. *Geophysical Prospecting*, 68(2), 591-614.

[12] Jayalakshmi S, Dhanya J, Raghukanth STG, Mai PM (2020): 3D seismic wave amplification in the Indo-Gangetic basin from spectral element simulations. *Soil Dynamics and Earthquake Engineering*, 129, 105923.

[13] Cheng AHD, Badmus T, Beskos DE (1991): Integral equation for dynamic poroelasticity in frequency domain with BEM solution. *Journal of engineering mechanics*, 117(5), 1136-1157.

[14] Schanz M. (2001): Application of 3D time domain boundary element formulation to wave propagation in poroelastic solids. *Engineering Analysis with Boundary Elements*, 25(4-5), 363-376.

[15] Liang JW, Liu ZX (2009): Diffraction of elastic waves by a cavity in poroelastic half-space. *Earthquake Engineering and Engineering Vibration*, 8(1): 29-46.

[16] Liu ZX, Ju X, Wu CQ, Liang JW (2017): Scattering of plane P1 waves and dynamic stress concentration by a lined tunnel in a fluid-saturated poroelastic half-space. *Tunnelling and Underground Space Technology*, 67, 71-84.

[17] Meng ZJ, Cheng H, Ma LD, Cheng YM (2019): The hybrid element-free Galerkin method for three-dimensional wave propagation problems. *International Journal for Numerical Methods in Engineering*, 117(1), 15-37.

[18] Yoshida KI, Nishimura N, Kobayashi S (2000): Analysis of three dimensional scattering of elastic waves by a crack with fast multipole boundary integral equation method. *Journal of applied mechanics*, 3, 143-150.

[19] Lee J (2007): Earthquake site effect modeling in sedimentary basins using a three-dimensional indirect boundary element-fast multipole method. *Doctoral dissertation, State University of New York at Binghamton*.

[20] Liu ZX, Wu FJ, Wang D (2015): The multi-domain FMM-IBEM to model elastic wave scattering by three-dimensional inclusions in infinite domain. *Engineering Analysis with Boundary Elements*, 60, 95-105.

[21] Chaillat S, Darbas M, Le Louër F (2017): Fast iterative boundary element methods for high-frequency scattering problems in 3D elastodynamics. *Journal of Computational Physics*, 341, 429-446.

[22] Liu ZX, He CR, Wang HL, Sun SJ (2019): Two-dimensional FM-IBEM solution to the broadband scattering of elastic waves in a fluid-saturated poroelastic half-space. *Engineering Analysis with Boundary Elements*, 104: 300-319.

[23] Liu ZX, Sun SJ, Cheng AHD, Wang YR (2018): A fast multipole accelerated indirect boundary element method for broadband scattering of elastic waves in a fluid‐saturated poroelastic domain. *International Journal for Numerical and Analytical Methods in Geomechanics*, 42(18), 2133-2160.

[24] Sakuma T, Yasuda Y (2002): Fast multipole boundary element method for large-scale steady-state sound field analysis. Part I: setup and validation. *Acta Acustica united with Acustica*, 88(4), 513-525.

[25] Rokhlin V (1993): Diagonal forms of translation operators for the Helmholtz equation in three dimensions. *Applied and Computational Harmonic Analysis*, 1(1), 82-93.

[26] Liang JW, You HB, Lee VW (2006): Scattering of SV waves by a canyon in a fluid-saturated, poroelastic layered half-space, modeled using the indirect boundary element method. *Soil Dynamics and Earthquake Engineering*, 26(6-7), 611-625.

[27] Lin CH, Lee VW, Trifunac MD (2005): The reflection of plane waves in a poroelastic half-space saturated with inviscid fluid. *Soil Dynamics and Earthquake Engineering*, 25(3), 205-223.

